remote sensing

MDPI

Article

Statistical Characteristics of Raindrop Size Distribution in the Monsoon Season Observed in Southern China

Asi Zhang [1,2], Junjun Hu [3,*], Sheng Chen [1,2,*], Dongming Hu [4], Zhenqing Liang [5], Chaoying Huang [5], Liusi Xiao [1,2,4], Chao Min [1,2] and Haowen Li [4]

1 School of Atmospheric Sciences, and Guangdong Province Key Laboratory for Climate Change and Natural Disaster Studies, Sun Yat-sen University, Guangzhou 510275, China; zhangas@mail2.sysu.edu.cn (A.Z.); xiaoliusi104@163.com (L.X.); minch@mail2.sysu.edu.cn (C.M.)
2 Southern Laboratory of Ocean Science and Engineering, Zhuhai, Guangdong, China
3 Cooperative Institute for Mesoscale Meteorological Studies, The University of Oklahoma, Norman, OK 73019, USA
4 Guangzhou Meteorological Observatory, Guangzhou, Guangdong 511430, China; dongminghu1976@163.com (D.H.); lihaowen@mail3.sysu.edu.cn (H.L.)
5 School of Geography and Planning, Guangxi Teachers Education University, Nanning 530001, China; liangzhenqing163@163.com (Z.L.); huang.chaoying@163.com (C.H.)
* Correspondence: Junjun.Hu-1@ou.edu (J.H.); chensheng@mail.sysu.edu.cn (S.C.)

Received: 3 January 2019; Accepted: 15 February 2019; Published: 19 February 2019

Abstract: This study investigates the statistical characteristics of raindrop size distributions (DSDs) in monsoon season with observations collected by the second-generation Particle Size and Velocity (Parsivel^2) disdrometer located in Zhuhai, southern China. The characteristics are quantified based on convective and stratiform precipitation classified using the rainfall intensity and total number of drops. On average of the whole dataset, the DSD characteristic in southern China consists of a higher number concentration of relatively small-sized drops when compare with eastern China and northern China, respectively. In the meanwhile, the D_m and $\log_{10}N_w$ scatter plots prove that the convective rain in monsoon season can be identified as maritime-like cluster. The DSD is in good agreement with a three-parameter gamma distribution, especially for the medium to large raindrop size. Using filtered data observed by Parsivel^2 disdrometer, a new Z–R relationship, $Z = 498R^{1.3}$, is derived for convective rain in monsoon season in southern China. These results offer insights of the microphysical nature of precipitation in Zhuhai during monsoon season, and provide essential information that may be useful for precipitation retrievals based on weather radar observations.

Keywords: southern China; raindrop size distribution; monsoon season

1. Introduction

Raindrop size distribution (DSD) reflects the particle size distribution characteristics of raindrops and is a fundamental characterization of precipitation microphysics. This parameter is also highly related with microphysical process such as accretion, evaporation, and precipitation rate [1]. Many studies have shown that the DSD varies not only in space and time but also within a specific storm even in different types of storm and weather system [2–4]. Understanding the variability of DSD is essential for improving quantitative precipitation estimates (QPE) using weather radar and satellite observations since the radar reflectivity factor is proportional to the sixth moment and rain rate is approximately the 3.76th moment of raindrop diameter [5,6].

The accuracy of the QPE relies on the appropriateness of power law Z–R relationship as $Z = AR^b$, where Z represents the radar reflectivity factor for the single-polarization radar measurements and stands for reflectivity $Z_{h,v}$, differential reflectivity Z_{DR}, and specific differential phase K_{DP} for dual-polarization radar algorithm [7,8], and R is the rain rate. These variables in the above relations are obtained for different radar wavelengths mostly using disdrometer-derived consistency equation [9]. Disdrometer observations are very helpful for investigating the highly variable characteristic of the DSD, at least to provide point information of measurement [10]. They can also provide detailed information on DSD which is crucial not only for raindrop microphysics but also for the calibration of remote sensing system [11]. Three commonly used disdrometers, such as Joss and Waldvogel disdrometer (JWD) [12], Particle Size and Velocity (PARSIVEL) disdrometer (PD) [13], and the two-dimensional video disdrometer (2DVD) [14], have been extensively used in measuring DSD characteristics in previous studies. However, these disdrometer measurements are inevitably contaminated by instrument limitations [15], undersampling [16], physical variations [17], splashing [18], and environmental factors such as wind effects [19].

The DSDs in the monsoon season in southern China have received very limited investigation. Tang et al. [20] studied the DSD characteristics for stratiform and convective rain types in different climate regions (northern China and southern China), and found that the spectrums of DSD in these climate regions differ little for stratiform rain types but maximum number of drops is largest in southern China while the northern China has the widest spectrum width of DSD. Wu et al. [21] gave a comparison of DSD between the Tibetan Plateau and southern China: the rain rate oscillation is much more frequent is southern China. They also investigated the Z–R relationship in Tibetan Plateau and southern China, and the result showed that the Tibetan Plateau had a smaller coefficient A and higher exponent b. However, they did not analyze the statistical characteristics of the rain DSDs in the whole monsoon season which heavy precipitation episodes such as squall line and typhoons happen frequently in southern China during monsoon season (May to August). As reported in previous studies [3,22,23], the rain DSD is different in different locations and would vary in the same synoptic system. As a result, investigation of the microphysical characteristic of precipitation in this area is of great significance to improve the accuracy of QPE based on weather radar observations.

The paper is organized as follows. The analysis methods and datasets are described in Section 2. The statistical results and characteristic comparison of DSD from different rain types are presented in Section 3. Section 4 gives the summary and conclusions.

2. Analysis Methods and Datasets

2.1. Parsivel^2 Disdrometer and Dataset

The DSD data analyzed in this study were collected with the second-generation Particle Size and Velocity (Parsivel^2) disdrometer manufactured by OTT Messtechnik, Germany. The Parsivel^2 is an optical, laser-based device [13] providing simultaneous measurements of particle size and fall-speed of hydrometeors and integrated DSD parameters such as rain rate, radar reflectivity factor, and information on precipitation type [10]. The Parsivel^2 can produce a 54 cm^2 horizontal laser beam and consists of a transmitter and a receiver. A single photodiode converts the laser signal into an electric voltage. When there are no precipitation particles in the laser beam, the output voltage of the receiver is the largest. Precipitation particles shield part of the laser beam with their corresponding diameter when they passing through the beam, thus they reduce the output voltage. The drop diameter is determined by the magnitude of voltage drop. Because the drops larger than 1 mm are not spherical, the calculation of the equivolume diameter is based on different axis ratio relationship [24]. For drops between 1 and 5 mm, the axis ratio linearly varies from 1 to 0.7. For drops with a diameter larger than 5 mm, the axis ratio is set to 0.7 [25,26].

The Parsivel^2 disdrometer has been extensively used in measuring the drop size from 0.2 mm to 5 mm for liquid precipitation and 0.2 mm to 25 mm in diameter for solid precipitation. The fall

velocities range from 0.2 m s^{-1} to 20 m s^{-1}. The particle size and velocities are each divided into 32 nonequidistant size and velocity bins. The lowest two size classes, which correspond to size smaller than 0.2 mm, are not used because of their low signal-to-noise ratios. Detailed particle size class and velocity class are given in Yuter et al. [27].

The data selected for this study consist of 1-min DSD data that were measured by OTT Parsivel^2 disdrometer at Zhuhai, located at the mouth of the Pearl River, belonging to southern China (Figure 1), and deeply influenced by summer monsoons. The DSD data were collected continuously from June to September 2018. (There were a tropical depression happened on 27 August to 2 September so the data time spanned two days of September.) To minimize the potential instrument error and obtain reliable data for this research, each minute of DSD has been carefully processed. The following criteria have been employed in choosing data for analysis. (1) Samples with 1-min total number of raindrops less than 10 or a disdrometer-derived rain rate less than 0.1 mm h^{-1} were regarded as noise and excluded in the analyses, otherwise it is regarded as a rainy minute; (2) raindrops at a diameter of more than 8 mm were eliminated; and (3) an effective rain event is defined on the basis of 30 minutes or longer rain-free period between the two consecutive rainy minutes [20,28,29]. In other words, a rain event at least lasts for 30 minutes. Finally, the monsoon season events consisted of 1032 one-minute DSD samples.

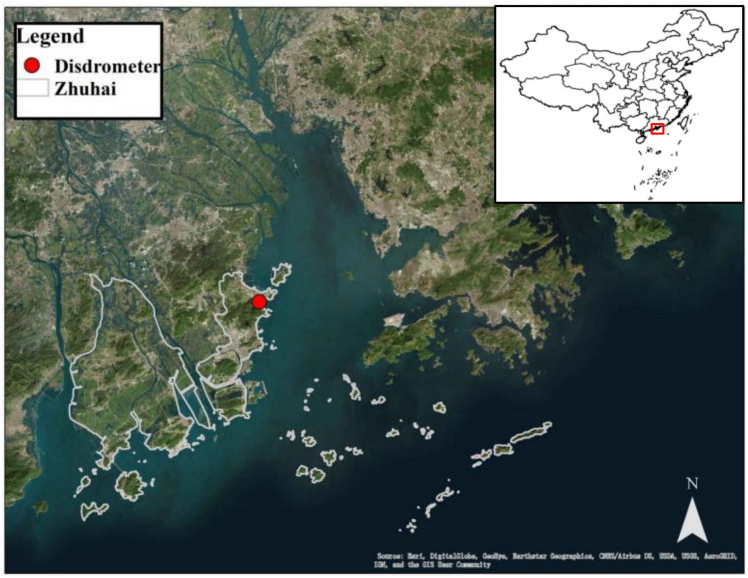

Figure 1. The map of Zhuhai. The red circle represents the disdrometer and the red rectangle is the rough location of Zhuhai in China.

2.2. Raindrop Size Distribution

The number concentration of raindrops per unit volume per unit size interval for raindrop diameter is calculated from the OTT Parsivel^2 disdrometer as follows.

$$\mathrm{N}(D_i) = \sum_{j=1}^{32} \frac{n_{ij}}{A \cdot \Delta t \cdot V_j \cdot \Delta D_i}, \quad (1)$$

where $N(D_i)$ (mm^{-1} m^{-3}) is the number concentration of raindrops per unit volume per unit size interval for raindrop diameter D_i (mm); n_{ij} the number of raindrops within the size bin i and velocity bin j; A(m^2) and Δt(s) are the sampling area and sampling time, respectively; and V_j (m s^{-1}) is the falling speed for velocity bin j. In this study, the falling speed measurements from OTT Parsivel^2

disdrometer are not used because of measurement error, particularly at faster fall speeds and larger size [26,30]. Instead, the model-based velocity relation is given [28] as follows.

$$\mathrm{V}(D_i) \;=\; 9.65 - 10.3\exp(-0.6D_i), \tag{2}$$

The integral rainfall parameters including the rain rate R (mm h^{-1}), radar reflectivity factor Z (mm^6 m^{-3}), and liquid water content W (g m^{-3}) can be derived from $N(D_i)$ as follows.

$$\mathrm{R} \;=\; \frac{6\pi}{10^4}\sum_{i\,=\,1}^{32}\sum_{j\,=\,1}^{32} V_j \mathrm{N}(D_i)D_i^3\Delta D_i, \tag{3}$$

$$\mathrm{Z} \;=\; \sum_{i\,=\,1}^{32}\mathrm{N}(D_i)D_i^6\Delta D_i, \tag{4}$$

$$\mathrm{W} \;=\; \frac{\pi}{6000}\sum_{i\,=\,1}^{32}\mathrm{N}(D_i)D_i^3\Delta D_i, \tag{5}$$

The mass-weighted mean diameter D_m (mm) is a generally used characteristic raindrop diameter which equals the ratio of the 4th to the 3rd moment of the DSD:

$$D_m = \frac{M_4}{M_3}, \tag{6}$$

where D^n stands for the nth-moment of the DSD, which is defined as

$$M_n = \int_0^\infty D^n N(D)\mathrm{dD} = \sum_{i=1}^{32}\mathrm{N}(D_i)D_i^n\Delta D_i, \tag{7}$$

The normalized intercept parameter N_w in the unit of mm^{-1} m^{-3} is computed from D_m:

$$N_w = \frac{4^4}{\pi\rho_w}\left(\frac{10^3 W}{D_m^4}\right), \tag{8}$$

where ρ_w (1.0 g cm^{-1}) is the density of water.

The three-parameter gamma distribution is most commonly accepted model in describing the measured raindrop spectra, and it is generally enough to describe the DSD fluctuations observed on small scale [31] and has the capability of describing a broader variation in DSD, which is expressed as

$$N(D) = N_0 D^{\mu}\exp(-\Lambda D), \tag{9}$$

where N_0 is the intercept parameter in a unit of m^{-3} mm$^{-1-\mu}$, μ is the shape parameter (dimensionless), and Λ is the slope parameter in a unit of mm^{-1} [17]. The three parameters in (9) are estimated from the second, fourth and sixth moments of the observed distribution using the method of moment (MM) in (7) which was recommended for practical use [32].

2.3. Classification of Rain Types

Precipitation is generally divided into two clearly distinguishable types: stratiform and convective. It is of great importance to classify the rain types as it is significant in observational, modeling, and in the remote sensing field [33]. Numerous DSD studies have been proposed by investigating the differences between stratiform and convective rain [29,33–36]. To deeply investigate the characteristics of the stratiform and convective precipitation type, a classification procedure, similar to that of Chen et al. [29] and Bringi et al. [34] was adopted. It classifies a sample of R at the instant t_i, $R(t_i)$, as for stratiform, if the values of R values from $t_i - N$ to $t_i + N$ lie in the range of 0.5 to 5 mm h^{-1} and their standard deviation is less than 1.5 mm h^{-1}; otherwise, the sample is classified as convective if the values of R from $t_i - N$ to $t_i + N$ greater than 5 mm h^{-1}. Samples $R(t_i)$ which belong neither to

stratiform nor convective cluster and will be excluded from the investigation. In this study, N is set to be five samples.

Figure 2 shows the frequency distribution of rain rates based on the datasets from June to September. After data processing using the above methods, there were 1032 rain spectra left and convective precipitation samples portioning the whole dataset (1032 samples) are only ~20% (206 samples). The frequency of occurrence of the total rainfall in all datasets is 80% below 5 mm h^{-1}, and only 3% for the rain rate in the range of 5 to 10 mm h^{-1}.

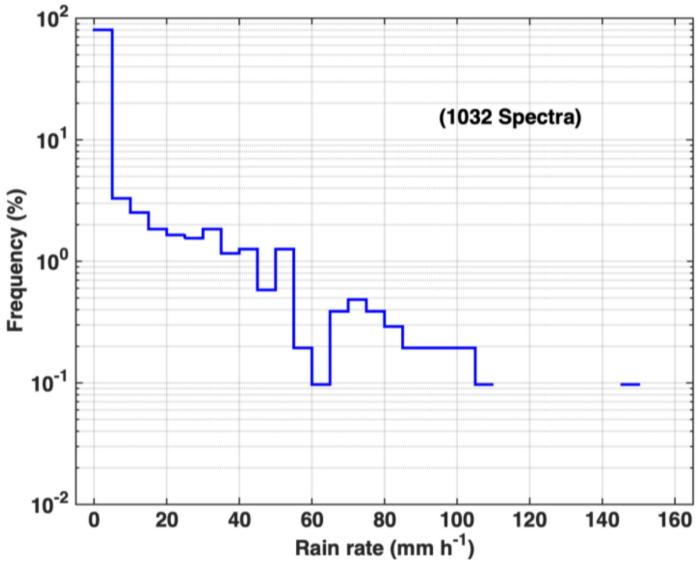

Figure 2. Frequency distribution of rain rates calculated from the whole OTT Parsivel^2 disdrometer datasets.

3. Results

3.1. Distribution of D_m and N_w

Figure 3 shows the relative frequency histogram of D_m and $\log_{10}N_w$ for the whole data set and for convective and stratiform subsets calculated from disdrometer. In addition, three key parameters, such as mean, standard deviation, and skewness, are used. As shown in Figure 3a, for the whole dataset, the mean value of D_m and $\log_{10}N_w$ is 1.46 mm and 3.86, respectively, which is similar to that of in eastern China (1.40 mm and 3.55, respectively) [29]. Note that the units of N_w are in mm^{-1} m^{-3}. The histogram of D_m has a highly positive skewedness, and on the contrary, the $\log_{10}N_w$ is slightly negatively skewed. The standard deviation of D_m and $\log_{10}N_w$ are large (0.46 mm and 0.5, respectively), indicating a high variability in D_m and N_w. When the whole datasets are classified into convective and stratiform, it can be found that the histogram means of D_m and $\log_{10}N_w$ from convective is 2.21 mm and 4.36, respectively, which is higher than that from stratiform precipitation (1.53 mm and 3.87, respectively). The convective histogram and stratiform histogram of D_m are both positively skewed (0.84 and 0.26); however, the $\log_{10}N_w$ histogram shows a negative skewness for convective (−1.33) and exhibits a positive skewness for stratiform precipitation (0.1). Averagely, it can be seen that the DSD characteristic in southern China consists of a higher number concentration when compared the results with eastern China [29] (3.86 versus 3.55 for $\log_{10}N_w$), and relatively small-sized drops as compared with northern China [37]. While compared to Darwin located in Australia, the DSD characteristic in southern China consists of a lower number concentration [38]. In addition to the altitude difference, the orographic effects in southern China cloud play an important part in the variability of DSD characteristic.

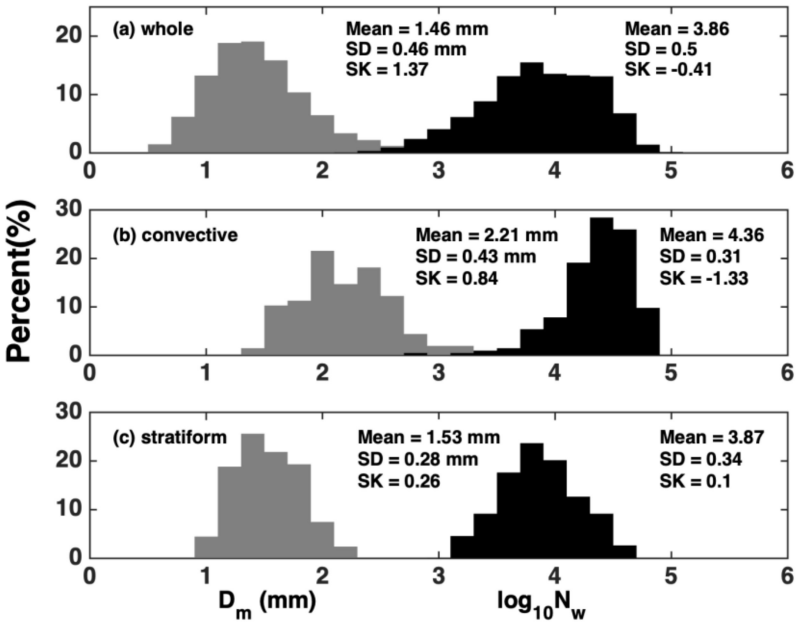

Figure 3. Histogram of D_m (left side) and $\log_{10}N_w$ (right side) for the (**a**) whole data set and (**b**) convective and (**c**) stratiform subsets calculated from the OTT Parsivel^2 disdrometer datasets.

Figure 4 shows the N_w versus R for the convective and stratiform rain events as derived from the OTT Parsivel^2 disdrometer. The red lines in Figure 4 are the fitted power law relationship calculated by a least-squares method. The points in Figure 4 are scattered, especially for convective rain type. Note that the exponent in the N_w–R relationship is positive, indicating that N_w is higher at higher rainfall rate, because of the more efficient mechanisms of coalescence and breakup process.

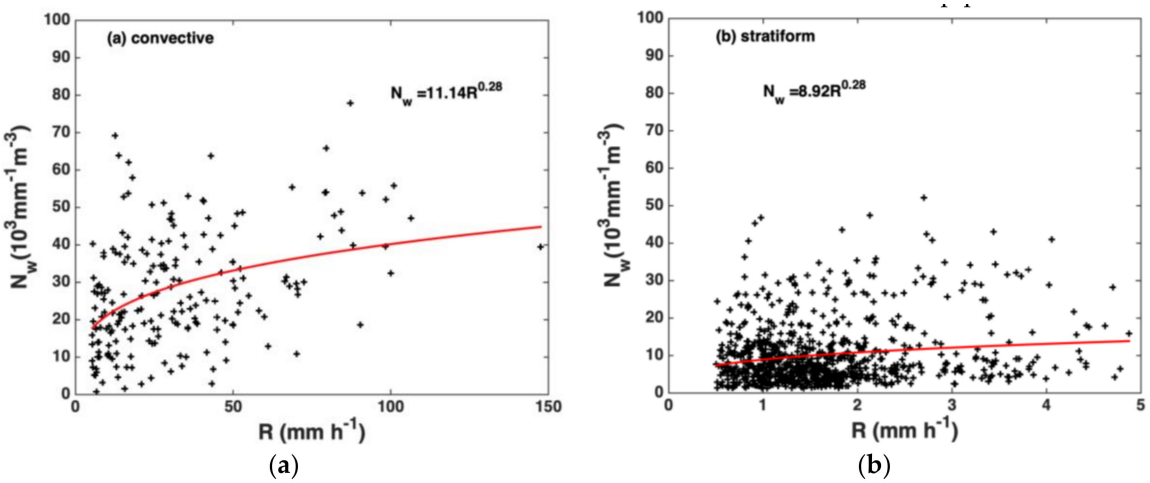

(**a**) (**b**)

Figure 4. Scatter plots of N_w vs. R for (**a**) convective and (**b**) stratiform rain types. The fitted power law relationships using a least-squares method are also provided in each panel.

Figure 5 shows the similar results expect for D_m versus R. However, the D_m-R plots are not as scattered as the N_w-R plots in Figure 4. At higher rain rate, the D_m values tend to be a stable value— ~2.5–3.0 mm for convective and 1.5–2.0 mm for stratiform rain types—indicating a tendency to equilibrium-like DSD [34]. With respect to the D_m-R relationship, the coefficient and exponent values of convective precipitation are slightly lower than stratiform, which has a diametrically opposed conclusion to Chen et al. [29] in eastern China. The climates in eastern and southern China are both deeply influenced by summer monsoons, which cause some similarities of the DSD characteristics in the two areas. Whereas, there are more typhoons landed in southern China which received more

than 500 mm annual typhoon precipitation, contributing ~20–40% of the total annual precipitation [39]. Research has been proven that the typhoon D_m is lower than that of non-typhoon values for different precipitation types also at all rain rates [40]. This could be the reason that the D_m-R is different between southern China and eastern China. In addition, the typhoon-related DSD characteristics are important to southern China QPE, which need further study in the future.

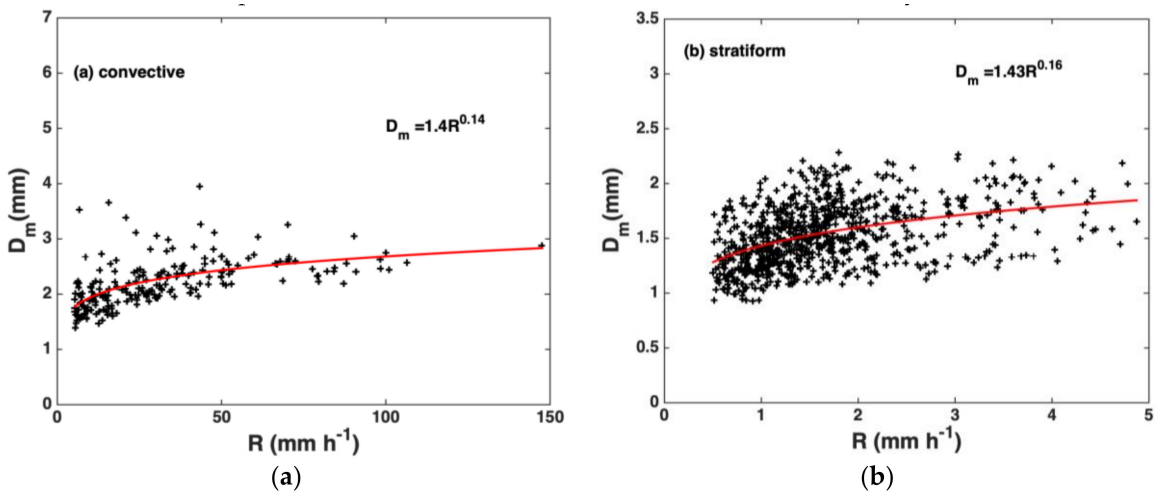

Figure 5. As in Figure 3, except for D_m versus R.

Figure 6 shows the distribution of the $\log_{10}N_w$ versus D_m derived from the disdrometer of two different rain types. The variability of N_w and D_m for stratiform is likely due to the different microphysical processes which are the melting of large dry snowflakes (larger D_m and smaller N_w) and the melting of tiny rimed snow particles (smaller D_m and larger N_w) [34]. In this study, the mean values of $\log_{10}N_w$ and D_m for stratiform are approximately 3.87 and 1.53 mm, respectively, as shown in Figure 3. This suggests that the melting of tiny, compact graupel, and rimed ice particles instead of melting of large dry snowflakes formed the stratiform rain type in southern China. Meanwhile, Figure 6 also illustrates a very clear separation of convective and stratiform rain types by a green dashed line in N_w-D_m domain. Here, the green separation line was drawn based on visual examination of the data with a slope of approximately −1.2097 and intercept of ~6.2434. Note that the separation line is different from that given in the equation (6) in the N_w-D_0 domain in the study by Bringi et al. [41]. The separation line given in [41] cannot work well in dividing the observations into convective and stratiform rain types.

Bringi et al. [34] found that in the case of convective rain, the maritime-like cluster has D_m ~ 1.5–1.75 mm and logarithmic N_w ~ 4–4.5 (gray rectangle in solid line) and the continental-like cluster has D_m ~ 1.5–1.75 mm and logarithmic N_w ~ 4–4.5 (gray rectangle in dashed line). As shown in Figure 5, only some of the convective N_w–D_m data are at the area of maritime convective cluster, and few of the data are observed in continental convective cluster. The mean values of logarithmic N_w and D_m calculated in Figure 3 are roughly in the maritime-like convective cluster. Note that the D_m is slightly higher than the maritime convective D_m values, implying the D_m of convective rain in monsoon season is larger as compare with maritime-like cluster. So far, the DSD characteristics are also studied at other places in China. Chen et al. [4] used the summer months of three years in Tibetan Plateau and found that convective rain at daytime could be identified as continental-like cluster while the night fall in the maritime-like cluster. Based on 96 rainfall events at the Shunyi national meteorological observation station located in northern China, Wen et al. [37] found that whether the convective DSDs can be characterized as maritime or continental-like cluster up to the orientations and mechanisms of rainfall system.

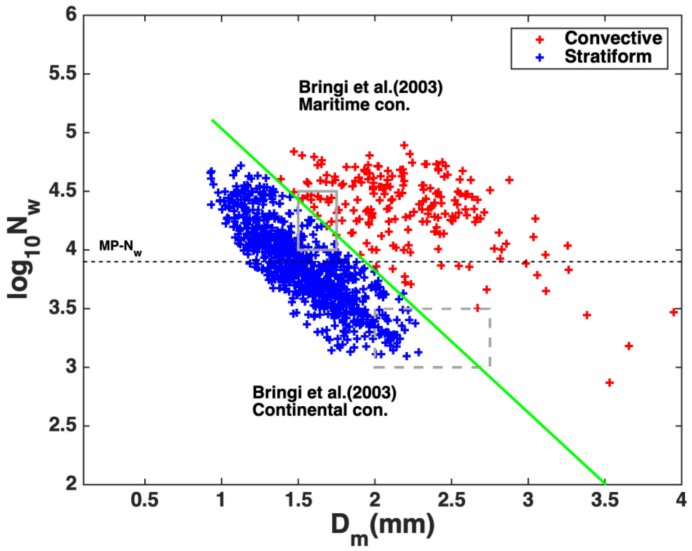

Figure 6. Scatter plot of D_m and $\log_{10}N_w$ for convective (red cross) and stratiform (blue cross) rain types. The two gray rectangles represent the maritime (solid line) and continental convective (dashed line) clusters by Bringi et al. (2003). The green line represents the separation line and was drawn based on visual examination of the data.

3.2. Composite Raindrop Spectra

Further, we investigate the characteristic DSDs for convective and stratiform precipitation systems to understand the precipitation microphysical processes. Figure 7 is a composite raindrop spectrum for convective and stratiform rain and its fittings to the three parameter gamma distribution models. The red line is the gamma function fitted on convective spectrum using the second, fourth and sixth moment method and the blue line is for the stratiform spectrum. The integral physics parameters are calculated in Table 1. Generally, the gap between the convective and stratiform becomes wider as the rain drop diameters increasing and the width of convective rain type is larger than stratiform. When compared with stratiform, the convective has a higher concentration nearly at all size bins corresponding to a higher number concentration, more rain water content and higher rain rate (Table 1). The measured raindrop size distribution can be better described by a three-parameter gamma distribution especially for the medium to large raindrop sizes.

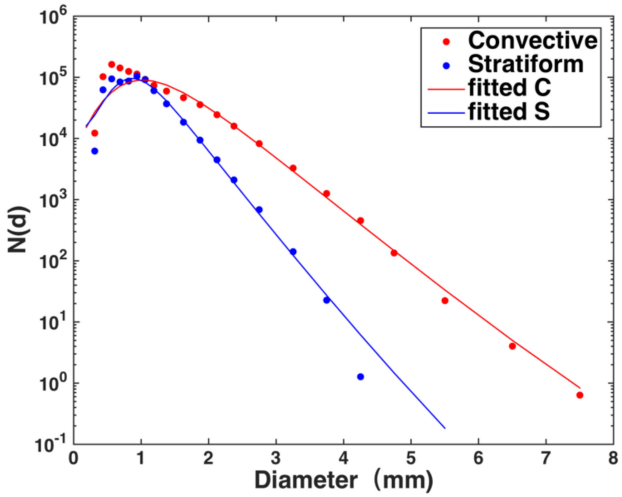

Figure 7. Composite raindrop spectrum for convective and stratiform rain types. The red line is the gamma function fitted on convective spectrum using the second, fourth and sixth moment method and the blue line is for the stratiform spectrum.

Table 1. Integral physics parameters derived from the composite raindrop spectra for different rain types [1].

Rain Type	N_T (m^{-3})	$\log_{10}N_w$ (N_w in m^{-3} mm^{-1})	W (g m^{-1})	R (mm h^{-1})	D_m (mm)
Convective	758	4.36	8.07	32.65	2.21
Stratiform	111	3.87	0.52	1.66	1.53
All	156	3.86	1.07	3.98	1.47

[1] Parameters such as N_T, N_w, W, R, and D_m are the total number concentration, generalized raindrop concentration, rain water content, rain rate, and mass-weighted mean diameter, respectively.

3.3. Shape–Slope Relation

Apart from the statistical results, an empirical μ–Λ relationship of three-parameter Gamma DSD is also evaluated. A three-parameter gamma distribution has been widely used to characterize DSD variability in microphysical parameterization schemes. Besides, the derived μ–Λ relationship provides useful information to reflect characteristic of DSDs and describe the behavior of the DSD parameters [42]. Several studies have shown that the three parameters N_0, μ and Λ are not mutually independent, with an N_0-μ relationship found by Ulbrich [17] to retrieve the DSD parameters from reflectivity and attenuation, and μ–Λ relationship suggested by Zhang et al. [43] to retrieve DSDs from reflectivity and differential reflectivity. Using the summer time DSD data collected in Florida, an empirical μ–Λ relation for rain rate larger than 5 mm h^{-1}, and total raindrop counts more than 1000 using truncated moment method [5,31] is as follows.

$$\Lambda = 0.0365\mu^2 + 0.735\mu + 1.935, \tag{10}$$

what is more, it should be noted that there are other empirical μ–Λ relationships proposed based on the disdrometer observations of DSD due to the variabilities of μ–Λ relationship across different location and climatic regimes [44–47]. Therefore, the Z–R relationship should be localized in southern China. In this study, the corresponding μ–Λ relationship is given by

$$\Lambda = 0.031\mu^2 + 0.446\mu + 1.453, \tag{11}$$

The relationship is derived on the data filtering method suggested by Chen et al. [29] using convective DSD data with total raindrop numbers higher than 1000. Accordingly, we also compare the relationship with eastern China proposed by Chen et al. [26] as follows.

$$\Lambda = 0.0141\mu^2 + 0.550\mu + 1.776, \tag{12}$$

As it can be observed in Figure 8, the red solid line is the μ–Λ relationship using a polynomial least-square fit (Equation (11)). The red dashed line and black dashed line are from Chen et al. [29] and Zhang et al. [42], respectively. We can clearly see the difference among the three areas through the μ–Λ relationship. The fitted μ–Λ relationship in southern China and eastern China are very similar which could due to the locations belonging to the similar climatological region because of the Asian summer monsoon. However, the μ–Λ relationships of both southern and eastern China vary greatly from that in Florida, and the differences become larger with the increasing rain rates (higher Λ value). Ulbrich [17] found that the μ–Λ relationship could be given by the approximate expression: $\Lambda D_m = 4 + \mu$. As shown in Figure 8, the four gray solid lines correspond to D_m = 1.0, D_m = 1.5, D_m = 2.0, and D_m = 3.0. Compared to Florida fitted line, the fittings in southern and eastern China are both at higher D_m area, which means the DSDs in southern China have a higher D_m than that in Florida. The above conclusions have proven that the μ–Λ relationship varies with different locations.

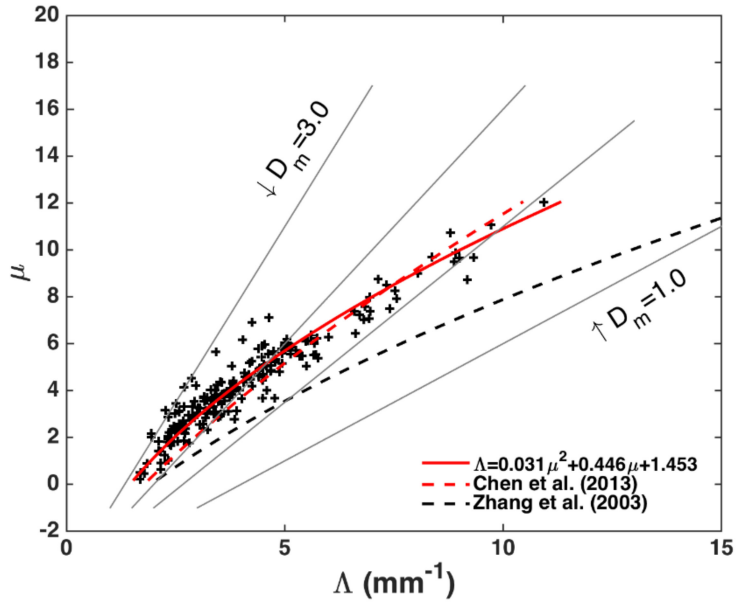

Figure 8. Scatter plot of μ–Λ values for convective rain obtained using the moment method and the truncated moment method with the filtering of total drop counts > 1000. The gray lines correspond to the relationship $\Lambda D_m = 4 + \mu$ given the values of D_m = 1.5, 2.0, 3.0, and 4.0 mm.

3.4. Z–R relationship

In this section, the empirical Z–R relationship ($Z = AR^b$) is analyzed by deriving R and Z from Equations (3) and (4) using a least-squares method. The values of A and b are closely related to the microphysical conditions of the DSD variations. Higher A values and lower b values are derived from convective mid-latitude precipitation, and on the contrary, lower A values and higher b values are applied for tropical precipitation [33]. Choosing the appropriate A and b based on different rain types has a great significance in improving the regional radar QPE. The relationship $Z = 300R^{1.4}$ is the convective precipitation relationship proposed by Fulton et al. [48] which is commonly applied in the standard NEXRAD (Next-Generation Weather Radar) Z–R relationship in the United States. The other relationship, $Z = 250R^{1.2}$, has been widely used to the tropical rainfall events [49]. Figure 9 shows that there is an appreciable difference on the coefficients A and b related to various regions. In order to compare the southern China Z–R relationship with other places, $Z = 368R^{1.2}$ for convective rain type in Meiyu season in eastern China, $Z = 300R^{1.4}$ for the standard NEXRAD in the United States and $Z = 250R^{1.2}$ for tropical precipitation are also provided. Compared to the standard Z–R relationship with A = 300 and b = 1.4, the fitted power law relationship in this study has a higher value of A = 498 and lower value of b = 1.3. Compared to the Z–R relationship derived from Meiyu season in eastern China, the monsoon season in southern China showed a higher A and b. Besides the parallel comparison with the above places, we also compare the Z–R relationship from Yangjiang [21], which is near our observation sites and has the same climatic regime and also has the similar coefficient and exponent ($Z = 526R^{1.3}$). In addition, for a given Z, the three power law relationships in the Figure 8 all overestimate rainfall, particularly the Z–R relationship at tropical areas.

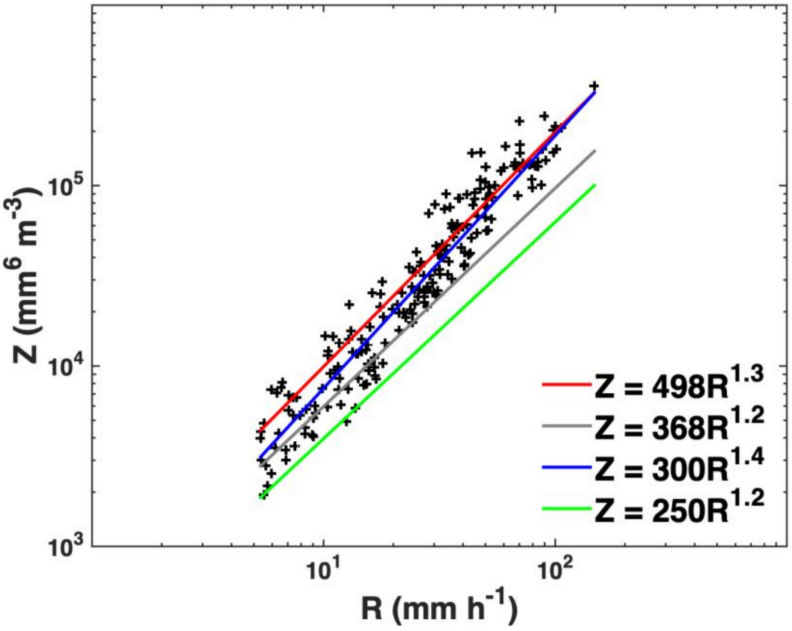

Figure 9. Scatter plot of Z versus R for convective rain observed from the filtered data only for the total drop counts > 1000. The fitted power law relationship in the form of $Z = AR^b$ using a least-squares method are shown in red line. The gray line stands for the Meiyu Z–R relationship in eastern China ($Z = 368R^{1.2}$), the blue line represents the standard NEXRAD Z–R relationship ($Z = 300R^{1.4}$), and the green line is the tropical Z–R relationship ($Z = 250R^{1.2}$).

4. Discussion

The statistical characteristics of DSD observed in monsoon season in southern China are documented using observations from the OTT Parsivel^2. The DSD observed by Parsivel^2 indicates that it consists of a higher number concentration compared with eastern China (Nanjing, Jiangsu). Despite both locations are influenced by a similar synoptic system in monsoon season, the altitude and orographic effects may be the primary reason to explain the difference. The DSD in Zhuhai is more like maritime-like cluster which also related to the location (see Figure 2). On the other hand, their Z–R relationship, derived from the disdrometer, is also different from other regions; previous research has shown that the coefficients may change with weather conditions, geographical location, and other possible reasons such as quality control and raindrop physical properties.

As aforementioned, the Parsivel^2 can only measure the drop size between 0.2 mm to 5 mm for liquid precipitation and 0.2 mm to 25 mm in diameter for solid precipitation, indicating that Parsivel^2 cannot detect the small drops with diameter less than 0.2 mm. Therefore, the readers need to keep in mind that the DSD measured by Parsivel2 in this study is not a complete DSD. Additionally, the other two commonly used disdrometers JWD and 2DVD also have limits on the sizes of raindrops that they can detect. Recent studies show that the 2DVD [14] can be used as reference instrument for the large end of the DSD [50,51] but underestimates concentrations of small drop with unreliable measurements under a drop diameter limit of 0.3 mm [52]. A study by Prat et al. [53] included that the JWD could not provide adequate measurement of the small drop end of the DSD. Recently, more and more efforts are reported to develop to adjust the disdrometer measurement of DSD aiming to overcome these limits of commonly used disdrometers [15,54,55]. Raupach and Berne [54] corrected the raindrop size distribution measured by Parsivel disdrometers using a 2DVD as reference. Thurai et al. [15,55] combined the DSD measurement from 2DVD and Meteorological Particle Spectrometer (MPS) to obtain more complete DSD spectra and developed a technique to reconstruct the drizzle mode of the DSD. The results shown in [15,55] indicate that the reconstruction technique of DSD drizzle mode is flexible and can obtain better rain rate estimations than previous DSD correction routine especially for

light rain. This has implication for DSD modelers and radar QPE developers as well as the numerical forecast modelers to give serious considerations of the drizzle mode in their research and applications.

5. Summary

Base on the DSD data observed with OTT Parsivel^2 disdrometer in Zhuhai, located in southern China, the characteristics of the DSD and calculated integral parameters are studied during the summer monsoon season. The main conclusions are as follows.

(1) The D_m histograms of both convective and stratiform are positively skewed, whereas the $\log_{10}N_w$ histograms have a negative skewness and positive skewness for convective and stratiform precipitation, respectively. What is more, the mean D_m and $\log_{10}N_w$ in convective rain are found to be higher than that of in stratiform rain (2.21 mm versus 1.53 mm for D_m and 4.36 versus 3.87 for $\log_{10}N_w$). On the average of the whole dataset, the DSD characteristic in southern China consists of a higher number concentration of relatively small-sized drops when compare with eastern China and northern China, respectively. Meanwhile, the D_m and $\log_{10}N_w$ scatter plot proves that the convective rain in monsoon season can be identified as maritime-like cluster.

(2) The averaged raindrop size distribution is in good agreement with a three-parameter gamma distribution especially for the medium to large raindrop size. The convective has a higher concentration almost at all size bins corresponding to a higher number concentration, more rain water content and higher rain rate. Retrievals of shape–slope parameter using the truncated moment method in both southern and eastern China vary greatly from that in Florida, and they also have a higher D_m than Florida.

(3) Using filtered data observed by the OTT Parsivel^2 disdrometer, a new Z–R relationship is derived for convective rain in monsoon season in southern China. Compared to the standard Z–R relationship with $Z = 300R^{1.4}$, the fitted power law relationship in southern China has a higher value of A = 498 and lower value of b = 1.3 ($Z = 498R^{1.3}$). Compared to the Z–R relationship derived from Meiyu season in eastern China ($Z = 368R^{1.2}$), the monsoon season showed higher A and b. Whereas the three power law relationships all overestimate rainfall, particularly the Z–R relationship at tropical areas ($Z = 250R^{1.2}$).

Statistic characteristics of DSD is very useful not only for weather forecast modelers to improve the numerical modeling of microphysical process of rain formation and evaluation but also for QPE developers to improve the accuracy of QPE products related to radar measurement of the precipitation, particularly in an era of dual polarization weather radar and global precipitation measurement mission with dual-frequency phased-array precipitation radar as a core instrument. This study first time reveals the characteristics of DSD measured by the Parsivel^2 at the Pearl River Estuary where the low-level jet from Western Pacific Ocean passes at monsoon season to trigger heavy precipitation in inland regions like Guangzhou city and far beyond. Such DSD information is helpful for local meteorological departments to improve the weather forecast service with more accurate weather forecast and real time radar QPE. However, as aforementioned, the Parsivel^2 has limitation in measuring small drops when compared to 2DVD and MPS. With the recent development of DSD modeling, it is necessary to obtain more complete DSD measurement via more accurate instrument like 2DVD and MPS. Also, the reconstruction technique of drizzle mode [15,55] can be tried in this region. This work will be conducted soon in coming future.

Author Contributions: The work presented here was carried out in collaboration with all authors. A.Z., S.C., and J.H. conceived and designed the content of this paper, D.H. designed the deployment of the disdrometer, L.X., C.H., Z.L., and C.M. helped setup disdrometer and process data, H.L. helped process and analyze data, S.C. and J.H. contributed to the reviewing and revising of the manuscript, and A.Z performed the calculation and wrote the manuscript.

Funding: This research was partially sponsored by the "100 Top Talents Program" (74110-52601108) at Sun Yat-sen University, Guangzhou, Guangdong, China; the High-Level Talents Training and Teacher Qualities and Skills Promotion Plan for Guangxi Colleges and Universities (8844); and by the National Natural Science Foundation of China (41875182, 51579162, 41661021, 41866001), Guangxi Natural Fund of Innovative Team Project (2016JJF15001).

Acknowledgments: Thanks are given to Long Wen and Hao Huang from Nanjing University, China for their help in processing the rain drop observations by OTT PARSIVEL^2. The authors also thank Guifu Zhang for his helpful suggestion for this study.

Conflicts of Interest: The authors declare no conflicts of interest.

References

1. Zhang, G.; Sun, J.; Brandes, E.A. Improving Parameterization of Rain Microphysics with Disdrometer and Radar Observations. *J. Atmos. Sci.* **2006**, *63*, 1273–1290. [CrossRef]
2. Jung, S.-A.; Lee, D.-I.; Jou, B.J.-D.; Uyeda, H. Microphysical Properties of Maritime Squall Line Observed on June 2, 2008 in Taiwan. *J. Meteorol. Soc. Jpn.* **2012**, *90*, 833–850. [CrossRef]
3. Ulbrich, C.W.; Atlas, D. Microphysics of Raindrop Size Spectra: Tropical Continental and Maritime Storms. *J. Appl. Meteorol. Climatol.* **2007**, *46*, 1777–1791. [CrossRef]
4. Chen, B.; Hu, Z.; Liu, L.; Zhang, G. Raindrop Size Distribution Measurements at 4,500 m on the Tibetan Plateau During TIPEX-III. *J. Geophys. Res. Atmos.* **2017**, *122*, 11092–11106. [CrossRef]
5. Vivekanandan, J.; Zhang, G.; Brandes, E. Polarimetric Radar Estimators Based on a Constrained Gamma Drop Size Distribution Model. *J. Appl. Meteorol.* **2004**, *43*, 217–230. [CrossRef]
6. Marshall, J.S.; Palmer, W.M.K. The Distribution of Raindrops with Size. *J. Meteorol.* **1948**, *5*, 165–166. [CrossRef]
7. Tokay, A.; Kruger, A.; Krajewski, W.F.; Kucera, P.A.; Filho, A.J.P. Measurements of drop size distribution in the southwestern Amazon basin. *J. Geophys. Res.* **2002**, *107*. [CrossRef]
8. You, C.-H.; Kang, M.-Y.; Lee, D.-I.; Uyeda, H. Rainfall estimation by S-band polarimetric radar in Korea. Part I: Preprocessing and preliminary results. *Meteorol. Appl.* **2014**, *21*, 975–983. [CrossRef]
9. Ryzhkov, A.V.; Giangrande, S.E.; Schuur, T.J. Rainfall Estimation with a Polarimetric Prototype of WSR-88D. *J. Appl. Meteorol.* **2005**, *44*, 502–515. [CrossRef]
10. Jaffrain, J.; Studzinski, A.; Berne, A. A network of disdrometers to quantify the small-scale variability of the raindrop size distribution. *Water Resour. Res.* **2011**, *47*. [CrossRef]
11. Marzano, F.S.; Cimini, D.; Montopoli, M. Investigating precipitation microphysics using ground-based microwave remote sensors and disdrometer data. *Atmos. Res.* **2010**, *97*, 583–600. [CrossRef]
12. Joss, J.; Waldvogel, A. Ein Spektrograph für Niederschlagstropfen mit automatischer Auswertung. *Pure Appl. Geophys.* **1967**, *68*, 240–246. [CrossRef]
13. Löffler-Mang, M.; Joss, J. An Optical Disdrometer for Measuring Size and Velocity of Hydrometeors. *J. Atmos. Ocean. Technol.* **2000**, *17*, 130–139. [CrossRef]
14. Schönhuber, M.; Lammer, G.; Randeu, W.L. One decade of imaging precipitation measurement by 2D-video-distrometer. *Adv. Geosci.* **2007**, *10*, 85–90. [CrossRef]
15. Raupach, T.H.; Thurai, M.; Bringi, V.N.; Berne, A. Reconstructing the drizzle mode of the raindrop size distribution using double-moment normalization. *J. Appl. Meteorol. Clim.* **2018**, *58*, 145–164. [CrossRef]
16. Gertzman, H.S.; Atlas, D. Sampling errors in the measurement of rain and hail parameters. *J. Geophys. Res.* **1977**, *82*, 4955–4966. [CrossRef]
17. Ulbrich, C.W. Natural Variations in the Analytical Form of the Raindrop Size Distribution. *J. Clim. Appl. Meteorol.* **1983**, *22*, 1764–1775. [CrossRef]
18. Angulo-MartÌnez, M.; BeguerÌa, S.; Fern·ndez-Raga, M.; Latorre GarcÈs, B. Comparison of precipitation measurements by OTT Parsivel2 and Thies LPM optical disdrometers. *Hydrol. Earth Syst. Sci.* **2018**, *22*, 2811–2837. [CrossRef]
19. Nešpor, V.; Krajewski, W.F.; Kruger, A. Wind-Induced Error of Raindrop Size Distribution Measurement Using a Two-Dimensional Video Disdrometer. *J. Atmos. Ocean. Technol.* **2000**, *17*, 1483–1492. [CrossRef]
20. Tang, Q.; Xiao, H.; Guo, C.; Feng, L. Characteristics of the raindrop size distributions and their retrieved polarimetric radar parameters in northern and southern China. *Atmos. Res.* **2014**, *135–136*, 59–75. [CrossRef]

21. Wu, Y.; Liu, L. Statistical characteristics of raindrop size distribution in the Tibetan Plateau and southern China. *Adv. Atmos. Sci.* **2017**, *34*, 727–736. [CrossRef]
22. Tokay, A.; Short, D.A.; Williams, C.R.; Ecklund, W.L.; Gage, K.S. Tropical Rainfall Associated with Convective and Stratiform Clouds: Intercomparison of Disdrometer and Profiler Measurements. *J. Appl. Meteorol.* **1999**, *38*, 302–320. [CrossRef]
23. Thurai, M.; Gatlin, P.N.; Bringi, V.N. Separating stratiform and convective rain types based on the drop size distribution characteristics using 2D video disdrometer data. *Atmos. Res.* **2016**, *169*, 416–423. [CrossRef]
24. Jaffrain, J.; Berne, A. Experimental Quantification of the Sampling Uncertainty Associated with Measurements from PARSIVEL Disdrometers. *J. Hydrometeorol.* **2010**, *12*, 352–370. [CrossRef]
25. Battaglia, A.; Rustemeier, E.; Tokay, A.; Blahak, U.; Simmer, C. PARSIVEL Snow Observations: A Critical Assessment. *J. Atmos. Ocean. Technol.* **2010**, *27*, 333–344. [CrossRef]
26. Tokay, A.; Wolff, D.B.; Petersen, W.A. Evaluation of the New Version of the Laser-Optical Disdrometer, OTT Parsivel^2. *J. Atmos. Ocean. Technol.* **2014**, *31*, 1276–1288. [CrossRef]
27. Yuter, S.E.; Kingsmill, D.E.; Nance, L.B.; Löffler-Mang, M. Observations of Precipitation Size and Fall Speed Characteristics within Coexisting Rain and Wet Snow. *J. Appl. Meteorol. Clim.* **2006**, *45*, 1450–1464. [CrossRef]
28. Atlas, D.; Srivastava, R.C.; Sekhon, R.S. Doppler radar characteristics of precipitation at vertical incidence. *Rev. Geophys.* **1973**, *11*, 1–35. [CrossRef]
29. Chen, B.; Yang, J.; Pu, J. Statistical Characteristics of Raindrop Size Distribution in the Meiyu Season Observed in Eastern China. *J. Meteorol. Soc. Jpn.* **2013**, *91*, 215–227. [CrossRef]
30. Chen, H.; Chandrasekar, V.; Bechini, R. An Improved Dual-Polarization Radar Rainfall Algorithm (DROPS2.0): Application in NASA IFloodS Field Campaign. *J. Hydrometeorol.* **2017**, *18*, 917–937. [CrossRef]
31. Ulbrich, C.W.; Atlas, D. Rainfall Microphysics and Radar Properties: Analysis Methods for Drop Size Spectra. *J. Appl. Meteorol.* **1998**, *37*, 912–923. [CrossRef]
32. Cao, Q.; Zhang, G. Errors in Estimating Raindrop Size Distribution Parameters Employing Disdrometer and Simulated Raindrop Spectra. *J. Appl. Meteorol. Climatol.* **2009**, *48*, 406–425. [CrossRef]
33. Tokay, A.; Short, D.A. Evidence from Tropical Raindrop Spectra of the Origin of Rain from Stratiform versus Convective Clouds. *J. Appl. Meteorol.* **1996**, *35*, 355–371. [CrossRef]
34. Bringi, V.N.; Chandrasekar, V.; Hubbert, J.; Gorgucci, E.; Randeu, W.L.; Schoenhuber, M. Raindrop Size Distribution in Different Climatic Regimes from Disdrometer and Dual-Polarized Radar Analysis. *J. Atmos. Sci.* **2003**, *60*, 354–365. [CrossRef]
35. Maki, M.; Keenan, T.D.; Sasaki, Y.; Nakamura, K. Characteristics of the Raindrop Size Distribution in Tropical Continental Squall Lines Observed in Darwin, Australia. *J. Appl. Meteorol.* **2001**, *40*, 1393–1412. [CrossRef]
36. Testud, J.; Oury, S.; Black, R.A.; Amayenc, P.; Dou, X. The Concept of "Normalized" Distribution to Describe Raindrop Spectra: A Tool for Cloud Physics and Cloud Remote Sensing. *J. Appl. Meteorol.* **2001**, *40*, 1118–1140. [CrossRef]
37. Wen, G.; Xiao, H.; Yang, H.; Bi, Y.; Xu, W. Characteristics of summer and winter precipitation over northern China. *Atmos. Res.* **2017**, *197*, 390–406. [CrossRef]
38. Thurai, M.; Bringi, V.N.; May, P.T. CPOL Radar-Derived Drop Size Distribution Statistics of Stratiform and Convective Rain for Two Regimes in Darwin, Australia. *J. Atmos. Ocean. Technol.* **2010**, *27*, 932–942. [CrossRef]
39. Ren, F.; Wu, G.; Dong, W.; Wang, X.; Wang, Y.; Ai, W.; Li, W. Changes in tropical cyclone precipitation over China. *Geophys. Res. Lett.* **2006**, *33*. [CrossRef]
40. Deo, A.; Walsh, K.J.E. Contrasting tropical cyclone and non-tropical cyclone related rainfall drop size distribution at Darwin, Australia. *Atmos. Res.* **2016**, *181*, 81–94. [CrossRef]
41. Bringi, V.N.; Williams, C.R.; Thurai, M.; May, P.T. Using Dual-Polarized Radar and Dual-Frequency Profiler for DSD Characterization: A Case Study from Darwin, Australia. *J. Atmos. Ocean. Technol.* **2009**, *26*, 2107–2122. [CrossRef]
42. Zhang, G.; Vivekanandan, J.; Brandes, E.A.; Meneghini, R.; Kozu, T. The Shape–Slope Relation in Observed Gamma Raindrop Size Distributions: Statistical Error or Useful Information? *J. Atmos. Ocean. Technol.* **2003**, *20*, 1106–1119. [CrossRef]
43. Zhang, G.; Vivekanandan, J.; Brandes, E. A method for estimating rain rate and drop size distribution from polarimetric radar measurements. *IEEE Trans. Geosci. Remote Sens.* **2001**, *39*, 830–841. [CrossRef]

44. Brandes, E.A.; Zhang, G.; Vivekanandan, J. Comparison of Polarimetric Radar Drop Size Distribution Retrieval Algorithms. *J. Atmos. Ocean. Technol.* **2004**, *21*, 584–598. [CrossRef]
45. Cao, Q.; Zhang, G.; Brandes, E.; Schuur, T.; Ryzhkov, A.; Ikeda, K. Analysis of Video Disdrometer and Polarimetric Radar Data to Characterize Rain Microphysics in Oklahoma. *J. Appl. Meteorol. Climatol.* **2008**, *47*, 2238–2255. [CrossRef]
46. Wen, J.; Zhao, K.; Huang, H.; Zhou, B.; Yang, Z.; Chen, G.; Wang, M.; Wen, L.; Dai, H.; Xu, L.; et al. Evolution of microphysical structure of a subtropical squall line observed by a polarimetric radar and a disdrometer during OPACC in Eastern China. *J. Geophys. Res. Atmos.* **2017**, *122*, 8033–8050. [CrossRef]
47. Kumar, L.S.; Lee, Y.H.; Ong, J.T. Two-Parameter Gamma Drop Size Distribution Models for Singapore. *IEEE Trans. Geosci. Remote Sens.* **2011**, *49*, 3371–3380. [CrossRef]
48. Fulton, R.A.; Breidenbach, J.P.; Seo, D.-J.; Miller, D.A.; O'Bannon, T. The WSR-88D Rainfall Algorithm. *Weather Forecast.* **1998**, *13*, 377–395. [CrossRef]
49. Rosenfeld, D.; Wolff, D.B.; Atlas, D. General Probability-matched Relations between Radar Reflectivity and Rain Rate. *J. Appl. Meteorol.* **1993**, *32*, 50–72. [CrossRef]
50. Gatlin, P.N.; Thurai, M.; Bringi, V.N.; Petersen, W.; Wolff, D.; Tokay, A.; Carey, L.; Wingo, M. Searching for Large Raindrops: A Global Summary of Two-Dimensional Video Disdrometer Observations. *J. Appl. Meteorol. Climatol.* **2015**, *54*, 1069–1089. [CrossRef]
51. Thurai, M.; Bringi, V.N. Application of the Generalized Gamma Model to Represent the Full Rain Drop Size Distribution Spectra. *J. Appl. Meteorol. Climatol.* **2018**, *57*, 1197–1210. [CrossRef]
52. Tokay, A.; Petersen, W.A.; Gatlin, P.; Wingo, M. Comparison of Raindrop Size Distribution Measurements by Collocated Disdrometers. *J. Atmos. Ocean. Technol.* **2013**, *30*, 1672–1690. [CrossRef]
53. Prat, O.P.; Barros, A.P.; Williams, C.R. An Intercomparison of Model Simulations and VPR Estimates of the Vertical Structure of Warm Stratiform Rainfall during TWP-ICE. *J. Appl. Meteorol. Climatol.* **2008**, *47*, 2797–2815. [CrossRef]
54. Raupach, T.H.; Berne, A. Correction of raindrop size distributions measured by Parsivel disdrometers, using a two-dimensional video disdrometer as a reference. *Atmos. Meas. Tech.* **2015**, *8*, 343–365. [CrossRef]
55. Thurai, M.; Gatlin, P.; Bringi, V.N.; Petersen, W.; Kennedy, P.; Notaroš, B.; Carey, L. Toward Completing the Raindrop Size Spectrum: Case Studies Involving 2D-Video Disdrometer, Droplet Spectrometer, and Polarimetric Radar Measurements. *J. Appl. Meteorol. Climatol.* **2017**, *56*, 877–896. [CrossRef]